AGU PUBLICATIONS

Geophysical Research Letters

RESEARCH LETTER
10.1002/2017GL073028

Key Points:
- Influence of increase in sea surface temperature resolution in ERA-Interim data set investigated in Gulf Stream region
- Substantial change in atmospheric response consistent with the change in mean sea surface temperature gradient
- Results indicate the significance of resolution in determining the role of oceanic fronts on weather and climate

Supporting Information:
- Supporting Information S1

Correspondence to:
R. Parfitt,
rparfitt@whoi.edu

Citation:
Parfitt, R., A. Czaja, and Y.-O. Kwon (2017), The impact of SST resolution change in the ERA-Interim reanalysis on wintertime Gulf Stream frontal air-sea interaction, *Geophys. Res. Lett.*, *44*, doi:10.1002/2017GL073028.

Received 9 FEB 2017
Accepted 22 MAR 2017
Accepted article online 27 MAR 2017

The impact of SST resolution change in the ERA-Interim reanalysis on wintertime Gulf Stream frontal air-sea interaction

Rhys Parfitt[1,2], Arnaud Czaja[2], and Young-Oh Kwon[1]

[1]Physical Oceanography Department, Woods Hole Oceanographic Institution, Falmouth, Massachusetts, USA, [2]Department of Physics, Imperial College London, London, UK

Abstract This paper examines the sensitivity to a change in sea surface temperature (SST) resolution of the interaction between atmospheric and oceanic fronts in the Gulf Stream region in the ERA-Interim reanalysis data set. Two periods are considered, January 1979 to December 2001 (SST resolution 1°×1°) and December 2010 to February 2016 (SST resolution 0.05°×0.05°). The winter season from the latter 6 years of high-resolution SST is compared against six random periods of six wintertime seasons from the low-resolution SST period, to assess the robustness of the result against natural climate variability. In all comparisons, a significant change in frontal air-sea sensible heat flux exchange is found that is highly correlated to the change in mean SST gradient. This leads to both increases and decreases in occurrence of atmospheric fronts and mean precipitation of up to 30%. These results reemphasize the importance of high SST resolution in resolving the influence of oceanic fronts on weather and climate.

1. Introduction

The significant role of strong oceanic fronts of sea surface temperature (SST) for variability in the midlatitude climate system is well documented at a variety of different spatial resolutions [e.g., *Chelton et al.,* 2004; *Sampe and Xie*, 2007; *Minobe et al.,* 2008; *Nakamura et al.,* 2008; *Kwon et al.,* 2010; *Booth et al.,* 2012]. Nevertheless, the extent of this role is a question that is still very much under debate. A recent article however has provided evidence to suggest that the key physical mechanism by which these strong oceanic frontal zones exert their influence is through their interaction with sharp fronts of temperature in the atmosphere associated with migrating weather systems [*Parfitt et al.,* 2016]. In that study, a decrease in the magnitude of the Gulf Stream (GS) SST gradient (analogous to a decrease in resolution) resulted in up to 30% less cold fronts being identified across most of the GS front. A mechanism of "thermal damping and strengthening (TDS)" was proposed to explain the observed change (see Figure S1 in the supporting information). These atmospheric fronts are embedded in baroclinic systems that are known to set the time mean atmospheric state in frontal regions such as the GS [*O'Neill et al.,* 2015; *Parfitt and Czaja*, 2016]. Crucially, not only is TDS highly dependent on the resolution of the SST, but there are also suggestions that there may be a threshold resolution below which this mechanism cannot be resolved [*Smirnov et al.,* 2015; *Willison et al.,* 2013]. Indeed, the underrepresentation of ocean-atmosphere coupling in general has long been linked to underrepresentation of SST gradients [*Chelton,* 2005]. Given this, it is critical to identify any associated artifacts in reanalysis data sets due to their coarse SST resolution or a change of the SST resolution in time.

Further motivation is provided from recent sensitivity studies to differently resolved Kuroshio Extensions (KE) resulting from the SST changes in the European Centre for Medium-Range Weather Forecasts (ECMWF)-reanalysis (ERA)-Interim data set [*Masunaga et al.,* 2015, 2016]. These series of studies found considerable mesoscale imprints of the KE on the atmospheric boundary layer that were present for the reanalysis only where the prescribed SST resolution was high enough. The aim of this article is to investigate the impact of this changing SST resolution in the ERA-Interim data set on the interaction between oceanic and atmospheric fronts. The focus will be on the wintertime GS sector, an area of substantial SST gradient, and the region where the frequency of midlatitude atmospheric fronts is the largest [*Berry et al.,* 2011a]. In section 2, the data and methods used are presented. The results are presented in section 3, and a summary and discussion are provided in section 4.

2. Data and Method

ERA-Interim is a global atmospheric reanalysis data set [*Simmons et al.,* 2007; *Berrisford et al.,* 2009; *Dee et al.,* 2011] available from January 1979 to present, with spectral resolution T255 (~0.7°) available on a 0.75° × 0.75° longitude-latitude grid. In this study, 12-hourly fields (at 0000 UTC and 1200 UTC) of the horizontal winds and air temperature are used at a pressure level of 925 hPa. Also used in this study are the sensible heat flux, convective precipitation, and large-scale precipitation that are taken from short-range forecast accumulations at both 0000 UTC and 1200 UTC.

However, despite the atmospheric model resolution remaining constant throughout the whole data set, the prescribed SST data have been improved twice. Between January 1979 and December 2001 the SST resolution is 1.0° × 1.0°, whereas between January 2002 and January 2009 it is 0.5° × 0.5°. From February 2009 onward, the SST resolution has been 0.05° × 0.05°. This study seeks to assess sensitivity to SST resolution by comparing the 6 year wintertime period DJF (December–February, where the year denotes the December month—i.e., DJF2010 is December 2010, January 2011, and February 2011) 2010–2015 ("High-res" SST resolution 0.05° × 0.05°) against six randomly selected 6 year DJF wintertime seasons within the period January 1979 to December 2001 ("Low-res" SST resolution 1.0° × 1.0°). The comparison is repeated using the six different low SST resolution periods to assess the robustness of results independent of the phase of the natural climate variability, e.g., North Atlantic Oscillation. A summary is provided in Table 1. Figure 1a illustrates the difference in mean SST for Low-res sample *i*, $\overline{\mathrm{SST}_{(i)}} = \overline{\mathrm{SST}_{\text{low-res}(i)}} - \overline{\mathrm{SST}_{\text{high-res}}}$. The plots for the other Low-res samples are shown in the supporting information Figure S1. Although subtle differences exist between each of these plots, the dominant signal ($\overline{\Delta \mathrm{SST}} \sim \pm 2\mathrm{K}$) following the GS front is highly consistent among all six of them. Figure 1b illustrates the corresponding difference in the magnitude of the mean SST gradient, $\left|\overline{\nabla \mathrm{SST}_{\text{low-res}(i)}}\right| - \left|\overline{\nabla \mathrm{SST}_{\text{high-res}}}\right|$ for Low-res sample *i*. Again, the plots for the other Low-res samples are shown in supporting information Figure S1. As before, the magnitude and pattern of the differences are extremely similar for the six different comparisons. This illustrates a sizable permanent artifact in both the SST and the SST gradient that results from the change in the SST resolution regardless of the phase of the internal climate variability.

In order to assess the impact of this artifact on the regional frontal air-sea interaction, atmospheric frontal grid points are identified with the "*F* diagnostic" [*Sheldon*, 2015; *Parfitt et al.,* 2016]. Regions where $F = \frac{\zeta_{925}|\nabla T_{925}|}{\zeta_o|\nabla T_o|} > 1$ are those considered to be frontal grid points, where $|\nabla T_{925}|$ is the magnitude of the temperature gradient on the 925 hPa pressure level, ζ_{925} is the isobaric relative vorticity on that same pressure surface, ζ_o is the Coriolis parameter at 40°N, and $|\nabla T_o|$ is a typical scale for temperature gradient, 1 K/100 km. Cold fronts are identified via $\boldsymbol{u}_{925}.\nabla T_{925} > 0$, where $\boldsymbol{u}_{925}$ is the horizontal velocity at 925 hPa, as is commonly suggested [e.g., *Hewson*, 1998]. It is noted that a change in the *F* threshold preferentially selects stronger or weaker frontal regions but does not change the conclusions reached in this study.

3. Results

3.1. Change in Frequency of Cold Fronts

Figures 2a and 2b illustrate the frequency of all atmospheric fronts and cold fronts for the High-res period DJF 2010–2015, respectively, as a fraction of the total 6 year wintertime period. As can be seen from these two figures, the cold frontal frequency is the main contributor to the total frontal frequency. Indeed, this is as expected since other studies have shown the cold frontal frequency in the wintertime Gulf Stream region to be roughly twice as frequent as warm fronts [e.g., *Berry et al.,* 2011a]. For this reason, the remainder of the study focuses on cold fronts exclusively. Figure 2c depicts the cold frontal frequency for Low-res sample *i*, while the same plots for the other Low-res samples are shown in the supporting information Figure S3. For each sample, there is a broad frequency signal across the GS front of ~10% of the respective total 6 year wintertime period. However, there are subtle differences in both the magnitude and spatial structure, as one might expect from large-scale variability between each sample.

Figure 2d illustrates the percentage change in cold frontal frequency between the High-res period and Low-res sample *i* (i.e., Low-res sample-High res period, such that blue (red) indicates a higher (lower) frontal frequency in the High-res period). Corresponding plots for the other Low-res samples are shown in the

Table 1. A Summary of the Six Randomly Selected Wintertime Seasons From the Low SST Resolution Period and the 6 Year Wintertime High SST Resolution Period[a]

Samples	Years (for DJF Data)	(I) Correlation Coefficient	(II) Correlation Coefficient	(III) Correlation Coefficient
Low-res *i*	1983, 1985, 1986, 1987, 1992, and 1998		0.784	
Low-res *ii*	1979, 1980, 1981, 1983, 1990, and 1999	0.605	0.795	0.723
Low-res *iii*	1987, 1988, 1990, 1994, 1995, and 1996	0.690	0.791	0.655
Low-res *iv*	1981, 1985, 1987, 1988, 1997, and 1998	0.829	0.781	0.857
Low-res *v*	1980, 1989, 1990, 1992, 1993, and 1999	0.584	0.780	0.759
Low-res *vi*	1979, 1983, 1984, 1992, 1994, and 1997	0.703	0.757	0.784
High-res	2010, 2011, 2012, 2013, 2014, and 2015			

[a](I, II, and III) Spatial pattern correlations for the three different pairs of variables in the domain (28.5°–78°W, 31.5°–52.5°N). (I) The correlation coefficients between the frequency change for the Low-res sample *i* (Figure 2d) and the same quantity for the other Low-res samples (Figures S3f–S3j). (II) The correlation coefficients between the change in d*Q*/d*y* between each Low-res sample with the High-res period (Figures 3c and S4f–S4j) and the corresponding change in $\left|\overline{\nabla \mathrm{SST}_{\mathrm{low-res}(n)}}\right|$ (Figures 1b and S2f–S2j). (III) The correlation coefficients between the change in total precipitation for the Low-res sample *i* (Figure 4c) and the same quantity for the other Low-res samples (Figures S7f–S7j).

supporting information Figure S3. For all Low-res samples there is a strong decrease across the majority of the GS front, but with increases to the north and south, revealing the presence of a tripole pattern of change in the wider GS region. In each case, the magnitude of change present in each tripole branch is roughly the same, with absolute values up to 30%. This consistency between the six different comparisons demonstrates the robustness of the signal to natural large-scale variability. In fact, the spatial correlations

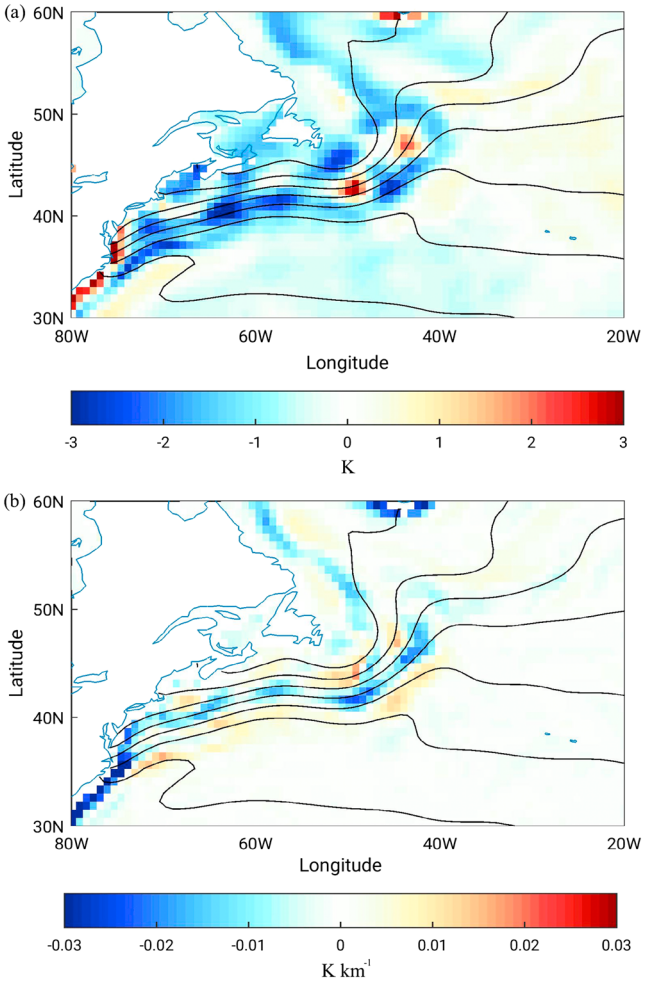

Figure 1. (a) The difference in mean SST between the High-res period and Low-res sample *i*, $\overline{\mathrm{SST}_{\mathrm{low-res}(i)}} - \overline{\mathrm{SST}_{\mathrm{high-res}}}$. (b) The corresponding difference in the magnitude of the mean SST gradient, $\left|\overline{\mathrm{SST}_{\mathrm{low-res}(i)}}\right| - \left|\overline{\nabla \mathrm{SST}_{\mathrm{high-res}}}\right|$. Mean SST contours for Low-res sample *i* are plotted from 3°C to 24°C, at 3°C intervals.

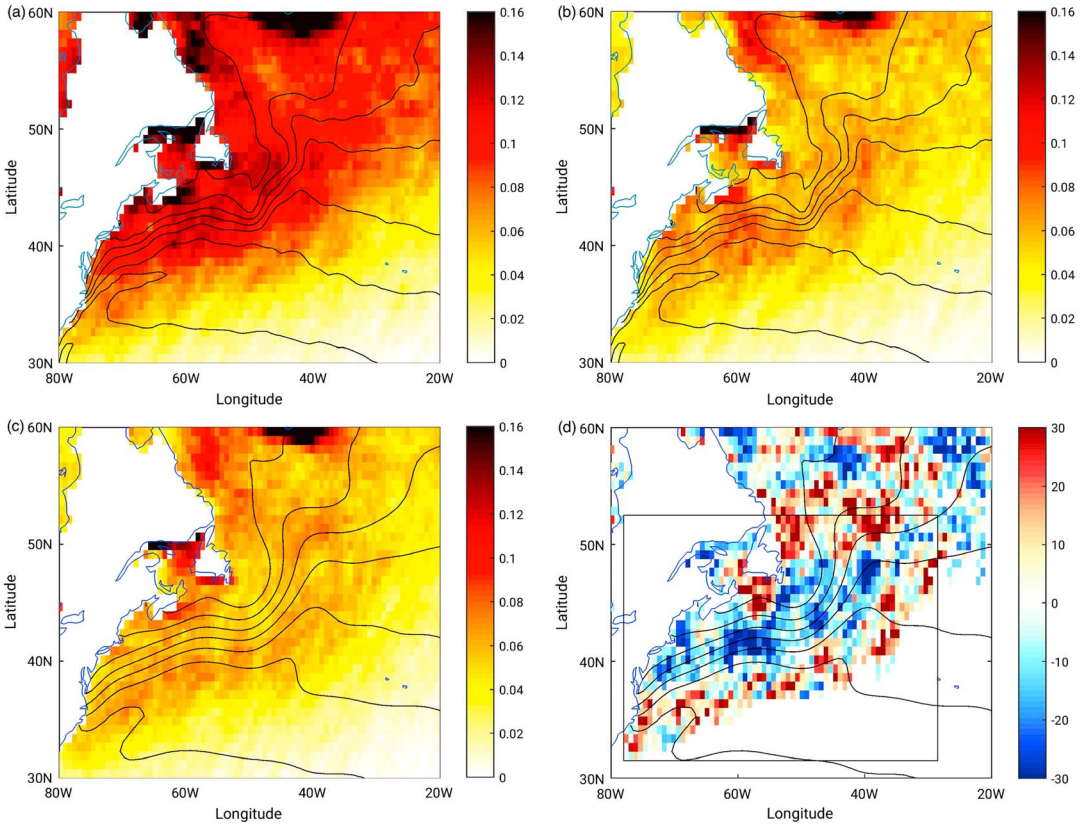

Figure 2. The frequency of (a) all atmospheric fronts and (b) cold fronts only, for the High-res period, as a fraction of the total 6 year High-res period. Mean SST contours for the High-res period are plotted from 3°C to 24°C, at 3°C intervals. (c) The cold frontal frequency for Low-res sample *i*. (d) The percentage change in cold frontal frequency between the High-res period Low-res sample *i*. The difference is calculated as the Low-res sample minus the High-res period, such that blue (red) indicates a higher (lower) frontal frequency in the High-res period. For Figures 2c and 2d, mean SST contours for Low-res sample *i* are plotted from 3°C to 24°C, at 3°C intervals. The rectangular black box in Figure 2d indicates the domain (28.5°–78°W, 31.5°–52.5°N).

between the percentage change in a GS rectangular domain (28.5°–78°W, 31.5°–52.5°N), for Low-res sample *i*, plotted in Figure 2d, and the percentage change in the same domain in each of the other Low-res samples show strikingly high values (Table 1(l)).

The broad decrease in cold frontal frequency of up to ~30% across the majority of the GS front is of a similar magnitude to that found in the previous study discussed in section 1 that investigated the sensitivity of cold frontal frequency to changing SST resolution in an atmospheric general circulation model (AGCM) across the GS region [*Parfitt et al.,* 2016]. The TDS mechanism, to which the changes in the AGCM experiments was attributed, is heavily tied to the how well the SST *gradient* is resolved, which primarily affects the strength of the air-sea sensible heat flux gradient across atmospheric fronts passing through the region. The next section addresses this issue further.

3.2. Change in Cross Cold-Frontal Sensible Heat Flux Gradient

Figure 3b illustrates the mean cross-frontal air-sea sensible heat flux gradient, d*Q*/d*y* (in Wm^{-2}/100 km, where *Q* is defined as positive when heat is released from the ocean into the atmosphere), experienced by cold atmospheric fronts at each location for the High-Res period DJF 2010–2015. More specifically, whenever a cold atmospheric front is identified at a location, a vector (*y*) that points perpendicularly toward the cold sector is established. The sensible heat flux gradient along that vector (across the front) is then calculated, and a composite mean at each location across the period is calculated. Because the gradient is defined positively toward the cold sector, wherever d*Q*/d*y* is positive (negative), the sensible heat flux gradient on average acts to thermally dampen (strengthen) the cold front, via TDS (supporting information Figure S1).

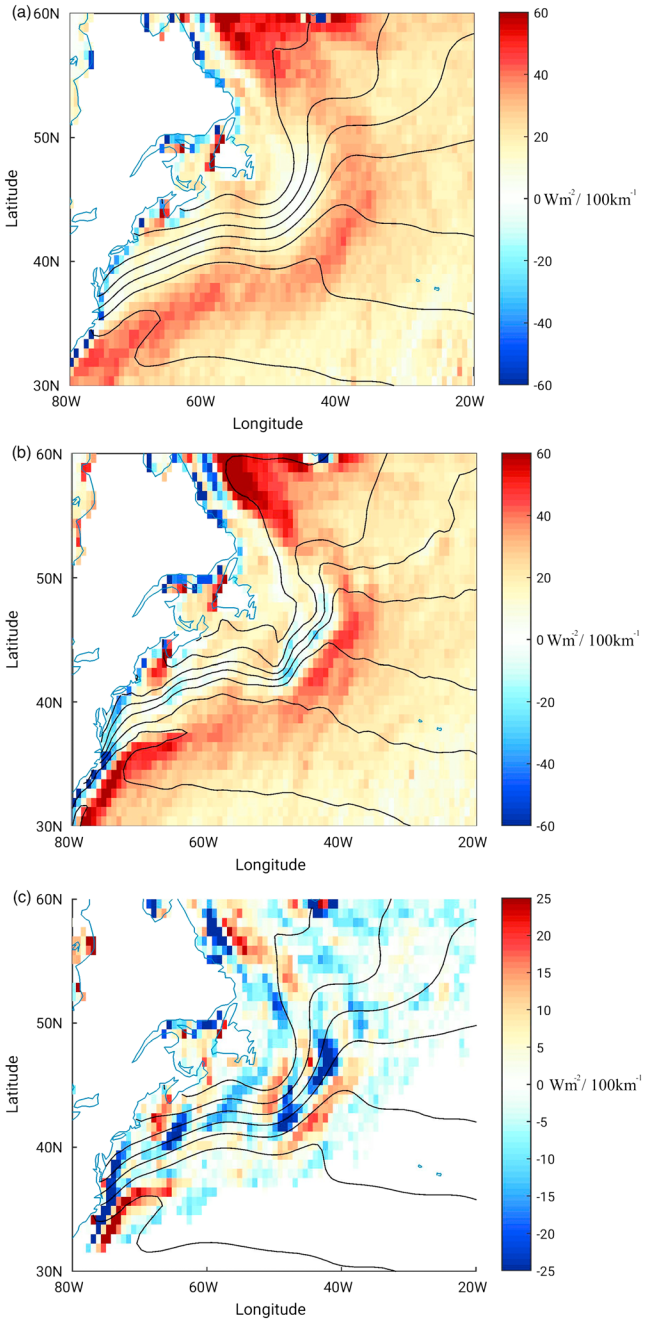

Figure 3. The average cross-frontal air-sea sensible heat flux gradient, d*Q*/d*y* (defined in the text), experienced by cold atmospheric fronts at each location for (a) Low-Res sample *i* and (b) the High-Res period. (c) The difference in magnitude between the High-res period and the 6 year Low-res sample *i*, calculated as the High-res period minus the Low-res samples (note that the sign convention is opposite to Figures 1 and 2), such that a negative (positive) difference implies that atmospheric cold fronts are on average dampened more (less) in the Low-res sample than in the High-res period. The mean SST contours from Low-res sample *i* are plotted from 3°C to 24°C, at 3°C intervals in Figures 3a and 3c, and those from the High-res period are in Figure 3b.

While in the region within the GS box but away from the GS front, the air-sea heat exchange acts to slightly dampen the cold fronts (~20 to 30 Wm^{-2}/100 km), a dipole exists across the GS front. To the north of the front there is a region where the air-sea heat exchange acts neutrally (~0 Wm^{-2}/100 km) or to strengthen the cold fronts (~−10 to −15 Wm^{-2}/100 km). To the south of the front however, there is a region of enhanced dampening (>40 Wm^{-2}/100 km). Such a distribution is strongly preferential to a pattern of intensification of passing atmospheric cold fronts that is aligned with the strong GS front. Figure 3a illustrates the analogous composite to Figure 3b but for Low-res sample *i*, with those for the remaining Low-res samples shown in the supporting information Figure S4. As in Figure 3a, in each Low-res sample for the region within the GS box but away from the GS front the tendency is for the air-sea heat exchange to moderately dampen the cold fronts (~20–30 Wm^{-2}/100 km), while a dipolar pattern exists across the GS front. However, there no longer exists a region along the GS front where the air-sea heat exchange acts neutrally or to strengthen the cold fronts. While to the south of the front there still exists a region of enhanced dampening (>40 Wm^{-2}/100 km), to the north there is now simply a region of weaker dampening (~10 Wm^{-2}/100 km). In other words, a less resolved GS front on average acts everywhere to dampen passing atmospheric cold fronts through air-sea sensible heat flux exchange. This phenomenon is consistent with that found in *Parfitt et al.* [2016].

Figure 3c shows the difference in magnitude between the High-res period and Low-res sample *i* (i.e., High-res period-Low-res sample), with the plots for the other Low-res samples shown in the supporting information Figure S4. Where this difference is negative (positive), atmospheric cold fronts are on average dampened more (less) in the Low-res sample than in the High-res period. Just off the continent exists a region of negative difference

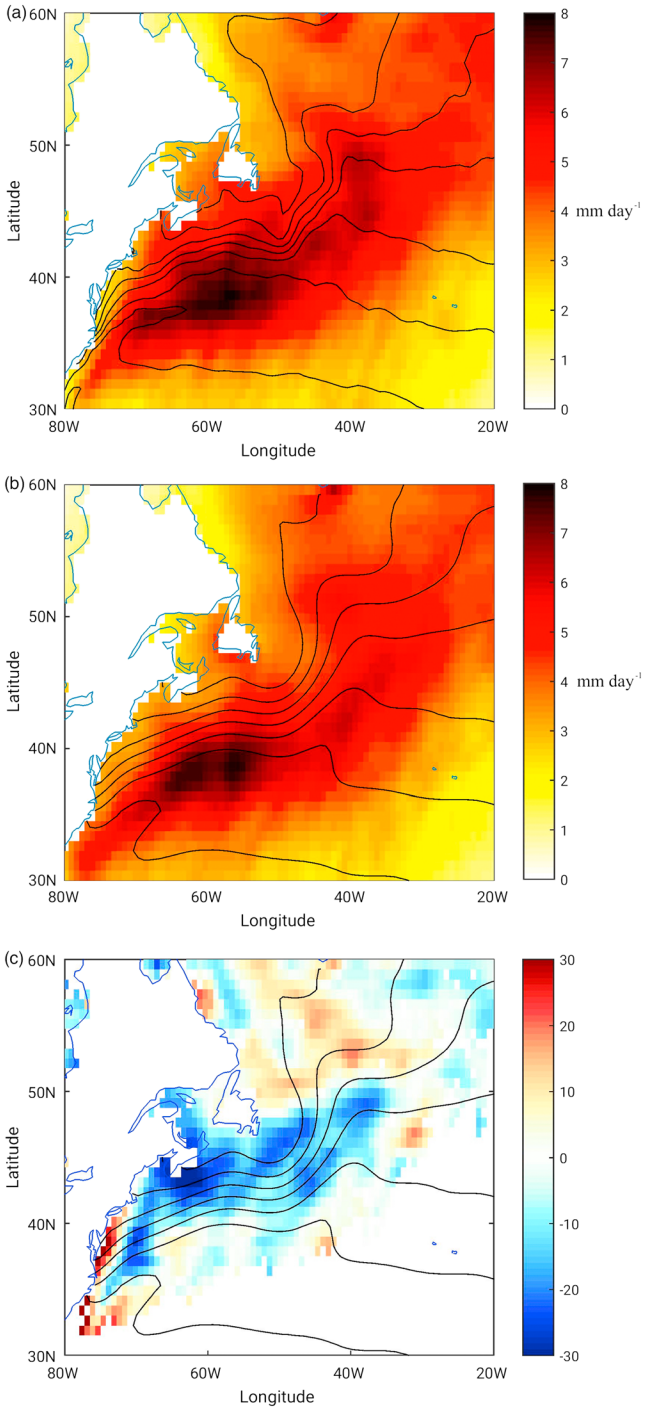

Figure 4. The mean total precipitation for (a) the High-res period and (b) Low-res sample *i*. (c) The percentage difference between the High-res period and Low-res sample *i*. This difference is calculated as 100 × (Low res-High res)/(High res) such that negative (positive) values imply more (less) precipitation in the High-res period. The mean SST contours from Low-res sample *i* are plotted from 3°C to 24°C, at 3°C intervals, in Figures 4b and 4c. The mean SST contours for the High-res period are plotted in Figure 4a.

that meanders with the GS front along the extent of the coast. All atmospheric cold fronts propagating off the continent across this region will therefore experience a stronger dampening in the Low-res samples than in the High-res period. As these storms travel on the order of $10\,m\,s^{-1}$ [*Neu et al.*, 2013], any thermal frontal air-sea interaction on a time scale of up to 1 day can potentially translate into a difference of up to roughly 10°. The slightly shifted spatial location and slightly broader region of cold frontal frequency decrease between 38° and 50°N shown in Figure 2d is thus not unexpected. This shifted spatial relationship is shown explicitly in the supporting information Figure S5. A corresponding shifted spatial relationship between weaker dampening and increased frontal frequency in the Low-res samples is also shown in the supporting information Figure S6. Outside of these regions this consistency is harder to highlight visually due to the complex structure of the change in d*Q*/d*y*. However, a spatial correlation in the GS rectangular domain (28.5°–78°W, 31.5°–52.5°N) of the difference in d*Q*/d*y* between each Low-res sample with the High-res period and the associated difference in $\left|\overline{\nabla SST_{low-res(n)}}\right|$ reveals a very high correlation (Table 1(II)). In other words, the changes in the gradient of air-sea sensible heat flux across atmospheric cold fronts that appear to be modulating the changes in the atmospheric cold frontal frequency in the region can be mostly explained by the change in the mean SST gradient between the Low-res samples and the High-res period.

3.3. Change in Total Precipitation

The observed impact of the change in SST gradient on atmospheric cold frontal frequency will naturally affect associated variables. An obvious example is the regional precipitation; in the Gulf Stream region extreme precipitation events are heavily biased toward frontal systems [*Parfitt and Czaja*, 2016]. Figure 4a illustrates the mean total precipitation

(convective and large scale) for the High-res period in mm d^{-1}, whereas Figure 4b shows the mean total precipitation for Low-res sample *i*. The mean total precipitation for each other Low-res sample is shown in supporting information Figure S7. While there is a general spatial structure in each Low-res sample that meanders with the GS front, there are subtle differences in both distribution and magnitude between them as one would expect from natural variability. However, Figure 4c, which illustrates the percentage difference between the High-res period and Low-res sample *i* shows that there is a broad decrease of up to 30% in total precipitation across the entire GS front, a signal which is echoed in each Low-res sample (supporting information Figure S7). It is noted that this percentage decrease, in terms of magnitude and general spatial structure, is seen almost equally in both the convective and large-scale precipitation separately (not shown). Indeed, the magnitude of this decrease in total precipitation is nearly the same as the broad decrease in atmospheric cold fronts observed in Figure 2 across the GS front. This relationship is perhaps not entirely unexpected, given that up to 90% of the total precipitation is associated with extratropical cyclones [*Hawcroft et al.,* 2012]. Once again, the consistency between the six different comparisons illustrates the robustness of this signal to large-scale variability (Table 1(III)). It is emphasized that to the north and south of this broad region of decrease are regions where the precipitation actually increases, consistent with the tripole pattern of cold frontal frequency change observed in Figure 2.

4. Summary and Discussion

This article has examined how sensitive the interaction between atmospheric and oceanic fronts in the wintertime Gulf Stream region is to SST resolution in the ERA-Interim reanalysis data set. Six random selections of six winter seasons (DJF) were selected from the Low-res period January 1979 to December 2001 and compared with 6 years from a High-res period DJF 2010–2015. In all six comparisons, the frequency of atmospheric cold fronts was reduced by up to 30% in the Low-res period across the GS front. To the north and south of the strongest SST gradient, an increase of up to 30% was present. The high correlation between the changes in each six comparisons indicates the robustness of the signal to natural variability. These magnitudes of change are also noticeably larger than those expected from any long-term trend [e.g., *Berry et al.,* 2011b]. Subsequent analysis of the changes in air-sea sensible heat flux gradient across those cold fronts revealed the frequency change to be consistent with the mechanism thermal damping and strengthening [*Parfitt et al.,* 2016]. This mechanism is highly dependent on how well both the atmospheric and oceanic fronts are resolved, and a spatial analysis between the changes in air-sea sensible heat flux gradient and the associated changes in SST gradient indeed revealed that both are highly correlated. It is duly noted however that other factors, such as the impact of the resolution change on vertical winds within the boundary layer, may also contribute to the magnitude and pattern of the frontal frequency change. As one might expect, the changes in the frequency of cold fronts are accompanied by corresponding changes in the surface storm-track activity (supporting information Figure S8, based on the definition of *Wallace et al.* [1988]). These results, along with other recent studies [e.g., *Parfitt et al.,* 2016], suggest that the impact of the SST gradient could potentially be stronger than that of the absolute SST in modulating passing storms, although the role of SST is still highly important [*Booth et al.,* 2012]. Furthermore, robust changes of up to 30% are also found in each of the six comparisons for the total precipitation, which are consistent with the structure and magnitude of change in the cold frontal frequency. This is to be expected given the high correlation between atmospheric cold fronts and precipitation along the midlatitude storm tracks, especially in the wintertime Gulf Stream region [*Catto et al.,* 2012].

All of the results in this study were reproduced for six additional low-resolution periods in which each period contained consecutive (rather than random) years, as well as 20 more distinct periods of six random years (not shown); in each case, the conclusions stay robust. It is noted that the 6 year High-res period has an average December–March North Atlantic Oscillation index [*Hurrell*, 1995] that is roughly the same as the median for the distribution of every possible 6 year Low-res sample, which minimizes any influence of large-scale interannual variability on these results (supporting information Figure S9).

Several recent studies have further hinted at the importance of SST gradient in the role that oceanic fronts play in affecting midlatitude weather and climate. For example, *Kwon and Joyce* [2013] showed that decadal variability in the Gulf Stream path has a significant effect on large-scale atmosphere variability, with associated anomalous patterns in SST gradient. Additionally, *Parfitt* [2014] illustrated that a change in the Gulf Stream SST gradient resulted in a "steering" of passing atmospheric fronts that noticeably changed

their direction of propagation by up to 10°. The results shown in this study further suggest an important role for the SST gradient in how oceanic fronts affect midlatitude weather and climate. One avenue currently being explored is the possibility of developing an oceanic index for western boundary currents specifically based on the SST gradient (e.g., the Oyashio Extension index used by *Frankignoul et al*. [2011] and *Kwon and Joyce* [2013]) or the surface heat flux exchange gradient, as opposed to other more traditionally used variables such as the sea surface height [e.g., *Qiu et al.,* 2014].

It is noted again that just as crucial as the SST gradient is the resolution of the SST data itself. Both are intimately connected as any change in the resolution will automatically affect the gradient. Given the magnitude of the artifacts in frontal frequency and precipitation observed in this study as a result of the change in SST resolution (and subsequently changes in SST gradient), caution must be taken when analyzing long-term trends in either reanalysis or model data sets within which the SST resolution changes or in making comparisons between two data sets in which the SST resolution is different. Indeed, it is emphasized that these artifacts exist in the ERA-Interim reanalysis despite the presence of data assimilation, meaning that the impact of the increase in SST resolution is rising above any assimilation constraints. Indeed, if the constraints were completely sufficient, one would expect to solely observe interannual variability. Furthermore, given recent studies that have suggested the interaction between atmospheric and oceanic fronts can only be properly considered at sufficiently high resolution [*Smirnov et al.,* 2015; *Parfitt et al.,* 2016], it is likely that an increasing impact of oceanic frontal zones on large-scale variability will be observed as the resolution of climate models increases. The exact magnitude, extent, and mechanism of this increase however is still an open question, and further research is presently being conducted by the authors using both high- and low-resolution coupled climate model simulations.

Acknowledgments
R.P. is funded by the Weston Howland Jr. postdoctoral scholarship at the Woods Hole Oceanographic Institution. Y.-O.K. is supported by NASA Physical Oceanography Program (NNX13AM59G) and DOE Regional and Global Climate Modeling Program (DE-SC0014433). The authors are grateful for the helpful comments of two anonymous reviewers. ERA-Interim is a public data set and is accessible online at http://apps.ecmwf.int/datasets. We would like to thank the ECMWF for allowing access to the data set.

References

Berrisford, P., D. P. Dee, K. F. Fielding, K. Fuentes, M. Kallberg, P. Kobayashi, and S. Uppala (2009), The ERA-Interim archive, ERA Rep. Ser., (1), 1–16.

Berry, G., M. J. Reeder, and C. Jakob (2011a), A global climatology of atmospheric fronts, *Geophys. Res. Lett.*, *38*, L04809, doi:10.1029/2010GL046451

Berry, G., C. Jakob, and M. Reeder (2011b), Recent global trends in atmospheric fronts, *Geophys. Res. Lett.*, *38*, L21812, doi:10.1029/2011GL049481.

Booth, J. F., L. Thompson, J. Patoux, and K. A. Kelly (2012), Sensitivity of midlatitude storm intensification to perturbations in the sea surface temperature near the Gulf Stream, *Mon. Weather Rev.*, *140*(4), 1241–1256.

Catto, J. L., C. Jakob, G. Berry, and N. Nicholls (2012), Relating global precipitation to atmospheric fronts, *Geophys. Res. Lett.*, *39*, L10805, doi:10.1029/2012GL051736.

Chelton, D. B. (2005), The impact of SST specification on ECMWF surface wind stress fields in the eastern tropical Pacific, *J. Clim.*, *18*(4), 530–550.

Chelton, D. B., M. G. Schlax, M. H. Freilich, and R. F. Milliff (2004), Satellite measurements reveal persistent small-scale features in ocean winds, *Science*, *303*(5660), 978–983.

Dee, D. P., et al. (2011), The ERA-Interim reanalysis: Configuration and performance of the data assimilation system, *Q. J. R. Meteorol. Soc.*, *137*(656), 553–597.

Frankignoul, C., N. Sennéchael, Y. O. Kwon, and M. A. Alexander (2011), Influence of the meridional shifts of the Kuroshio and the Oyashio Extensions on the atmospheric circulation, *J. Clim.*, *24*(3), 762–777.

Hawcroft, M. K., L. C. Shaffrey, K. I. Hodges, and H. F. Dacre (2012), How much Northern Hemisphere precipitation is associated with extratropical cyclones?, *Geophys. Res. Lett.*, *39*, L24809, doi:10.1029/2012GL053866.

Hewson, T. D. (1998), Objective fronts, *Meteorol. Appl.*, *5*(1), 37–65.

Hurrell, J. W. (1995), Decadal trends in the North Atlantic Oscillation: Regional temperatures and precipitation, *Science*, *269*, 676–679.

Kwon, Y. O., and T. M. Joyce (2013), Northern Hemisphere winter atmospheric transient eddy heat fluxes and the Gulf Stream and Kuroshio–Oyashio Extension variability, *J. Clim.*, *26*(24), 9839–9859.

Kwon, Y. O., M. A. Alexander, N. A. Bond, C. Frankignoul, H. Nakamura, B. Qiu, and L. A. Thompson (2010), Role of the Gulf Stream and Kuroshio-Oyashio systems in large-scale atmosphere-ocean interaction: A review, *J. Clim.*, *23*(12), 3249–3281.

Masunaga, R., H. Nakamura, T. Miyasaka, K. Nishii, and Y. Tanimoto (2015), Separation of climatological imprints of the Kuroshio Extension and Oyashio fronts on the wintertime atmospheric boundary layer: Their sensitivity to SST resolution prescribed for atmospheric reanalysis, *J. Clim.*, *28*, 1764–1787, doi:10.1175/JCLI-D-14-00314.1.

Masunaga, R., H. Nakamura, T. Miyasaka, K. Nishii, and B. Qiu (2016), Interannual modulations of oceanic imprints on the wintertime atmospheric boundary layer under the changing dynamical regimes of the Kuroshio Extension, *J. Clim.*, *29*(9), 3273–3296.

Minobe, S., A. Kuwano-Yoshida, N. Komori, S. P. Xie, and R. J. Small (2008), Influence of the Gulf Stream on the troposphere, *Nature*, *452*(7184), 206–209.

Nakamura, H., T. Sampe, A. Goto, W. Ohfuchi, and S. P. Xie (2008), On the importance of midlatitude oceanic frontal zones for the mean state and dominant variability in the tropospheric circulation, *Geophys. Res. Lett.*, *35*, L15709, doi:10.1029/2008GL034010.

Neu, U., et al. (2013), IMILAST: A community effort to intercompare extratropical cyclone detection and tracking algorithms, *Bull. Am. Meteorol. Soc.*, *94*(4), 529–547.

O'Neill, L. W., T. Haack, and E. Skyllingstad (2015), Intermittency of surface convergence over the Northwest Atlantic, Am. Meteorol. Soc. Ann. Meeting 2015, Phoenix, Ariz., 5–8 Jan. [Available at https://ams.confex.com/ams/95Annual/videogateway.cgi/id/29530?recordingid=29530.]

Parfitt, R. (2014), Extreme air-sea interactions over the Gulf Stream, 189 pp., PhD Thesis, Imperial College, London.

Parfitt, R., and A. Czaja (2016), On the contribution of synoptic transients to the mean atmospheric state in the Gulf Stream region, *Q. J. R. Meteorol. Soc.*, *142*, 1554–1561, doi:10.1002/qj.2689.

Parfitt, R., A. Czaja, S. Minobe, and A. Kuwano-Yoshida (2016), The atmospheric frontal response to SST perturbations in the Gulf Stream region, *Geophys. Res. Lett.*, *43*, 2299–2306, doi:10.1002/2016GL067723.

Qiu, B., S. Chen, N. Schneider, and B. Taguchi (2014), A coupled decadal prediction of the dynamic state of the Kuroshio Extension system, *J. Clim.*, *27*(4), 1751–1764.

Sampe, T., and S. P. Xie (2007), Mapping high sea winds from space, *Bull. Am. Meteorol. Soc.*, *88*(12), 1965.

Sheldon, L. (2015), The role of deep moist convective processes in western boundary currents-troposphere coupling, 229 pp., PhD thesis, Imperial College, London

Simmons, A., S. Uppala, D. Dee, and S. Kobayashi (2007), ERA-Interim: New ECMWF reanalysis products from 1989 onwards, *ECMWF Newslett.*, *110*(110), 25–35.

Smirnov, D., M. Newman, M. A. Alexander, Y.-O. Kwon, and C. Frankignoul (2015), Investigating the local atmospheric response to a realistic shift in the Oyashio sea surface temperature front, *J. Clim.*, *28*, 1126–1147.

Wallace, J. M., G. H. Lim, and M. L. Blackmon (1988), Relationship between cyclone tracks, anticyclone tracks and baroclinic waveguides, *J. Atmos. Sci.*, *45*(3), 439–462.

Willison, J., W. A. Robinson, and G. M. Lackmann (2013), The importance of resolving mesoscale latent heating in the North Atlantic storm track, *J. Atmos. Sci.*, *70*(7), 2234–2250.

Geophysical Research Letters

Supporting Information for

The impact of SST resolution change in the ERA-Interim reanalysis on wintertime Gulf Stream frontal air-sea interaction

Rhys Parfitt[1,2], Arnaud Czaja[2] and Young-Oh Kwon[1]

[1]Physical Oceanography Department, Woods Hole Oceanographic Institution
[2]Department of Physics, Imperial College London

Contents of this file

Figures S1 to S9

Introduction

This file contains Supplementary Figures 1-9, along with the associated captions.

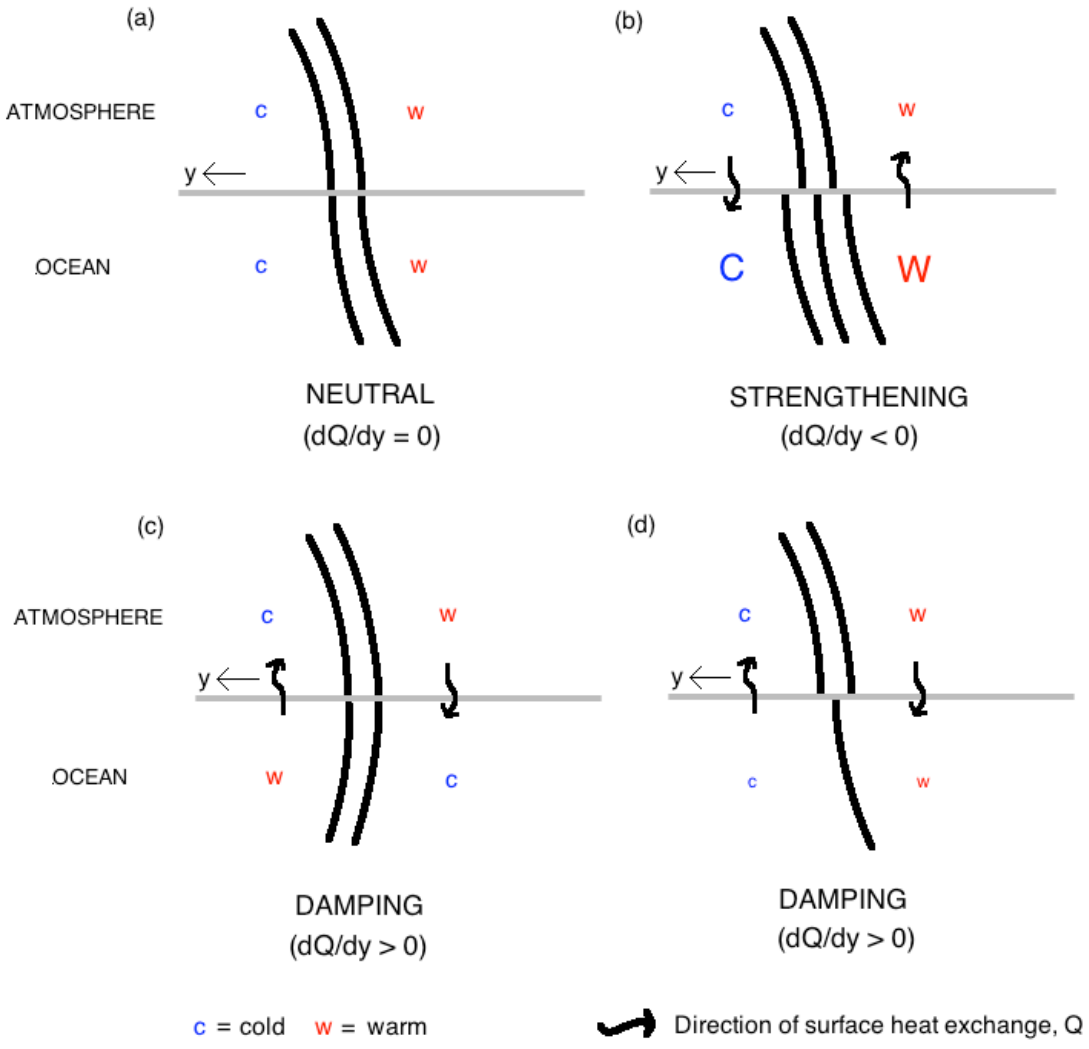

Figure S1. Schematic of an atmospheric cold front passing over (a) an SST gradient aligned such that the ocean temperature is equal to the atmospheric temperature at the surface, (b) a strong SST gradient aligned in the same direction, (c) an SST gradient aligned in the opposite direction and (d) a weak SST gradient aligned in the same direction. Black wavy arrows indicate the direction of surface sensible heat fluxes, while the cross-frontal direction vector (y) is shown as a thin black arrow (positive toward the cold sector). Perturbations in the magnitude of the cross-frontal surface sensible heat flux (as shown in these extreme cases), caused by a strengthening or a weakening of the SST gradient (b and d) or by changes in the relative orientation of atmospheric fronts (c) with the underlying oceanic fronts, are referred to as a 'Thermal Damping and Strengthening' mechanism. It is noted that the situation in (d) can also occur as a result of an insufficiently resolved ocean front.

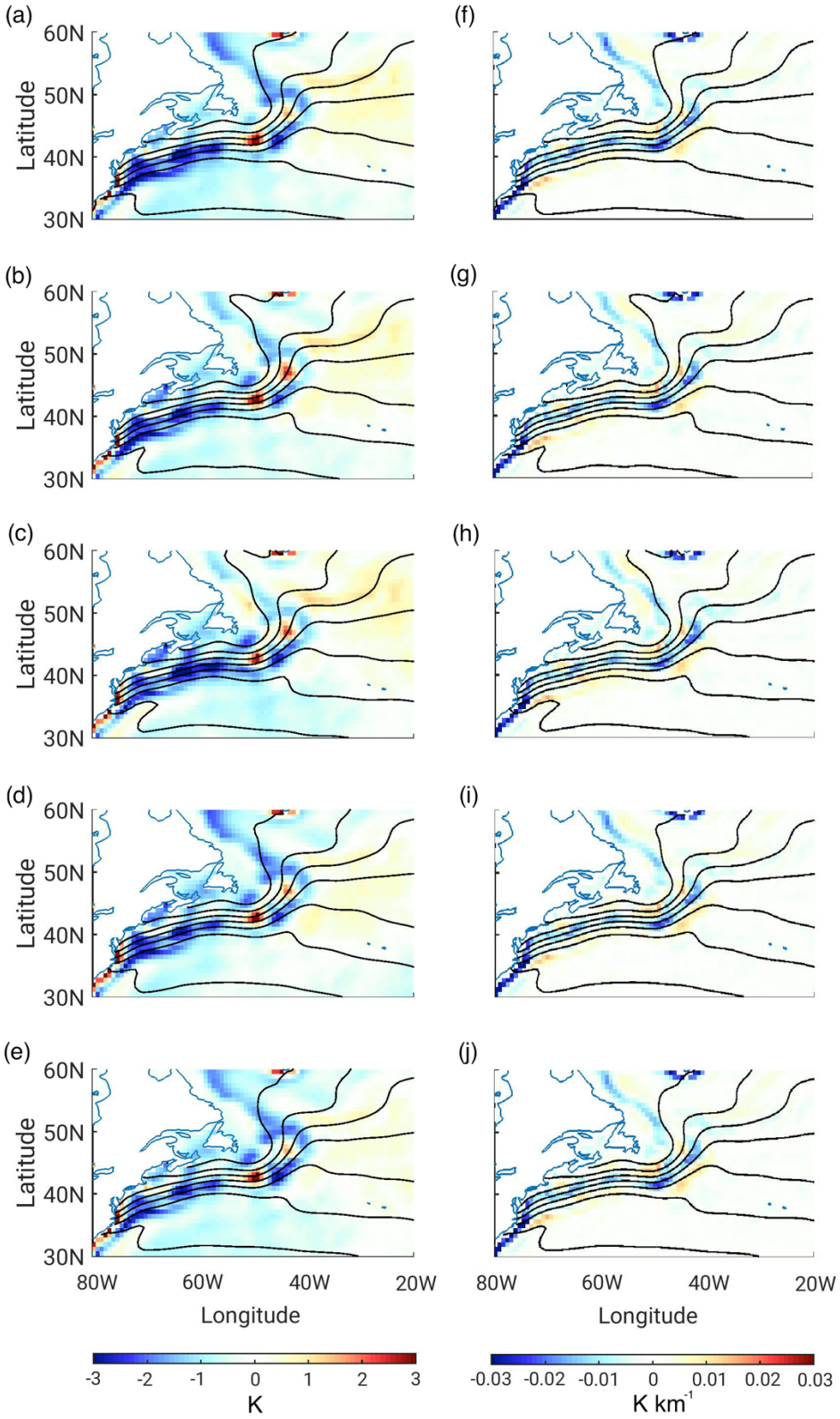

Figure S2. (a-e) The difference in mean SST between the High-res period and Low-res periods, $\overline{SST_{low-res(n)}} - \overline{SST_{high-res}}$, where $n = ii - vi$. (f-j) The difference in the magnitude of the mean SST gradient, $|\overline{VSST_{low-res(n)}}| - |\overline{VSST_{high-res}}|$ between the same periods. Mean SST contours for each corresponding Low-res period are plotted from 3°C to 24°C, at 3°C intervals.

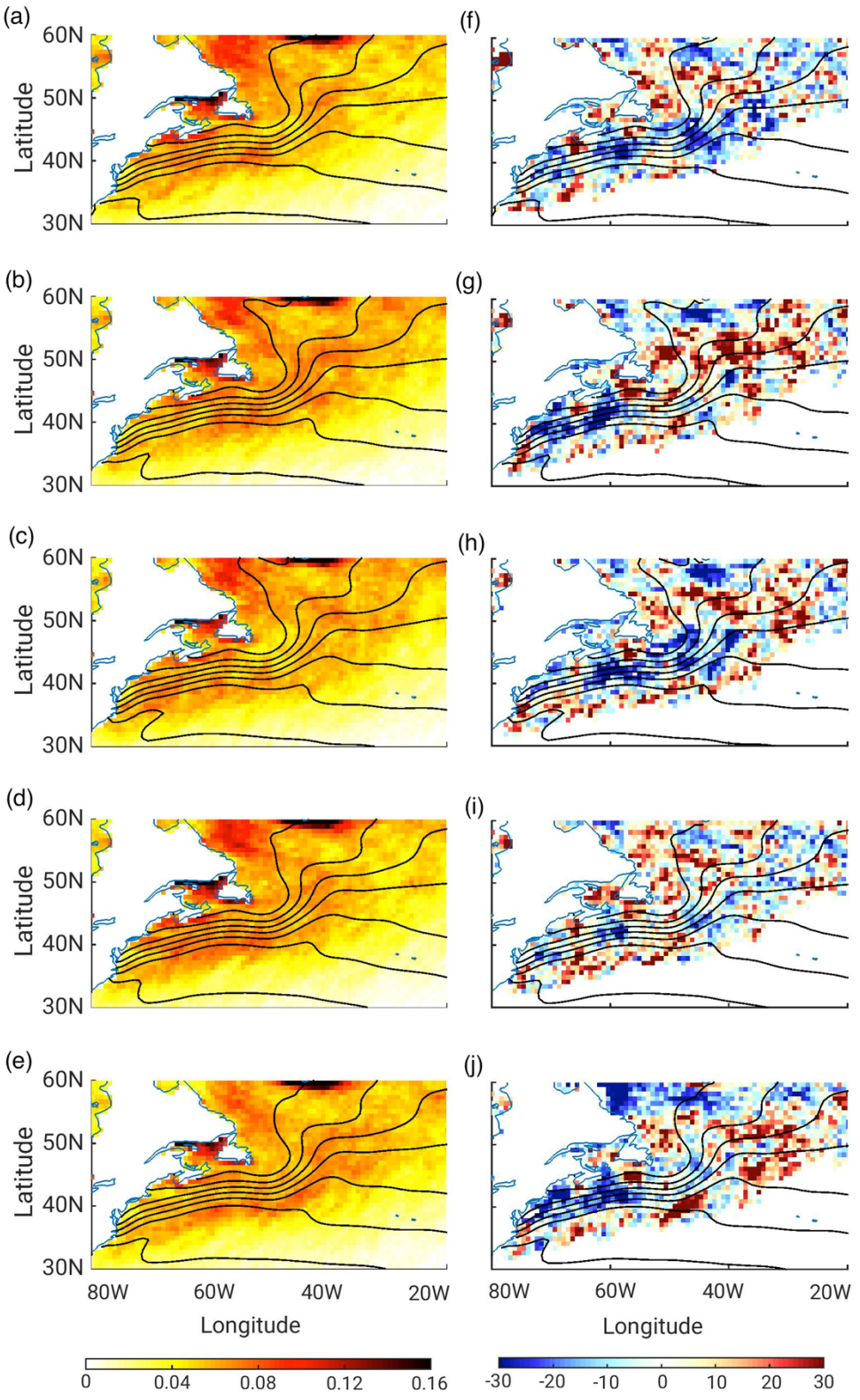

Figure S3: (a-e) The cold frontal frequency for each Low-res sample *ii*-*vi*, respectively. (f-j) The percentage changes in cold frontal frequency between the High-res period and each Low-res sample *ii*-*vi*, respectively. The difference is calculated as the Low-res samples minus the High res period, such that blue (red) indicates a higher (lower) frontal frequency in the High-res period. Mean SST contours from each corresponding Low-res period are plotted from 3°C to 24°C, at 3°C intervals.

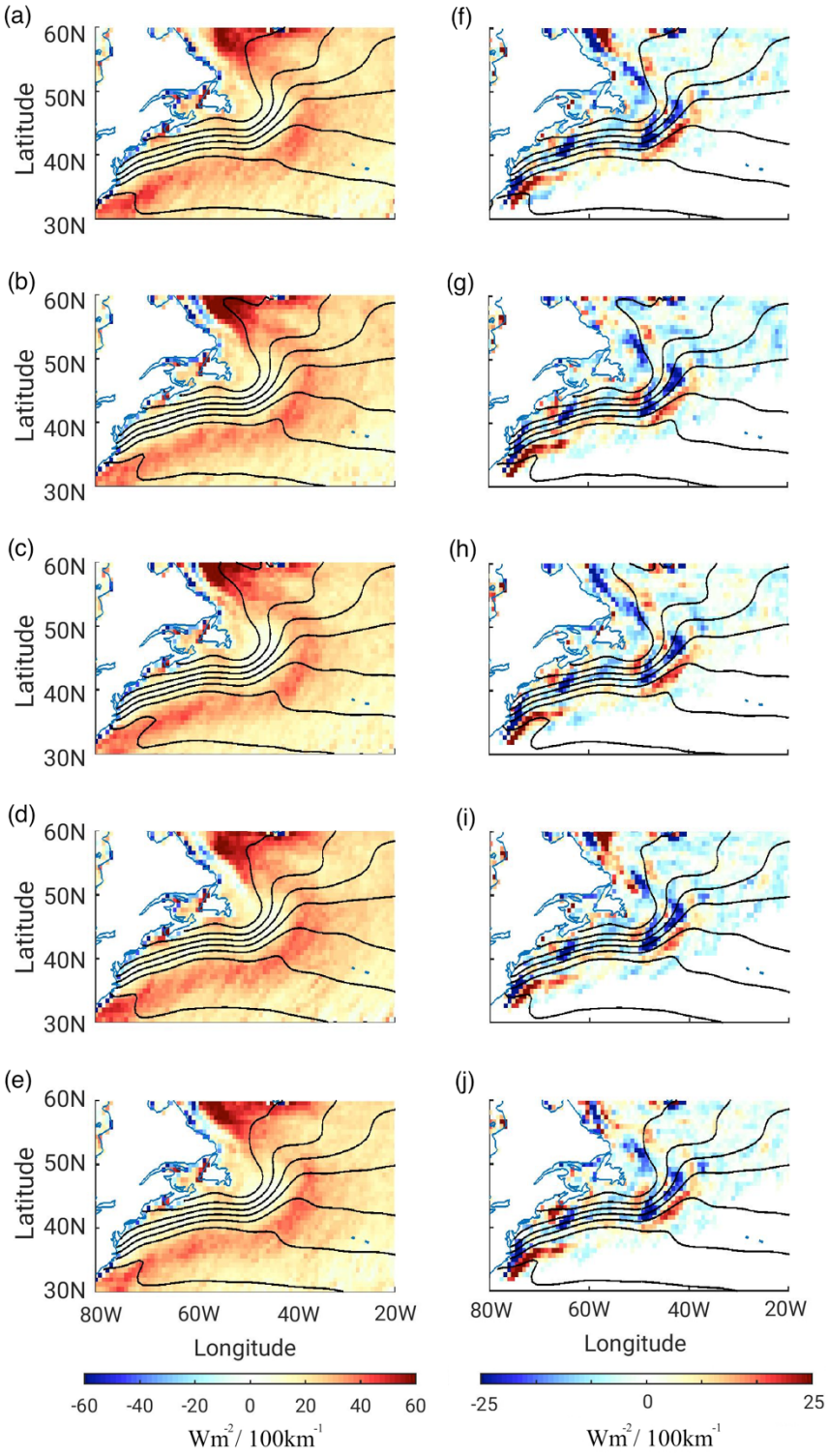

Figure S4: The average cross-frontal air-sea sensible heat flux gradient, dQ/dy (defined in the text), experienced by cold atmospheric fronts at each location for (a-e) Low-Res sample *ii-vi,* respectively. (f-j) The difference in magnitude between the High-res period and Low-res sample *ii-vi*, respectively, calculated as the High-res period minus the Low-res samples (note that the sign convention is opposite to the Figs. S1-S2), such that a negative (positive) difference implies that atmospheric cold fronts are on average dampened more (less) in the Low-res sample than in the High-res period. The mean SST contours from each corresponding Low-res period are plotted from 3°C to 24°C, at 3°C intervals in each panel.

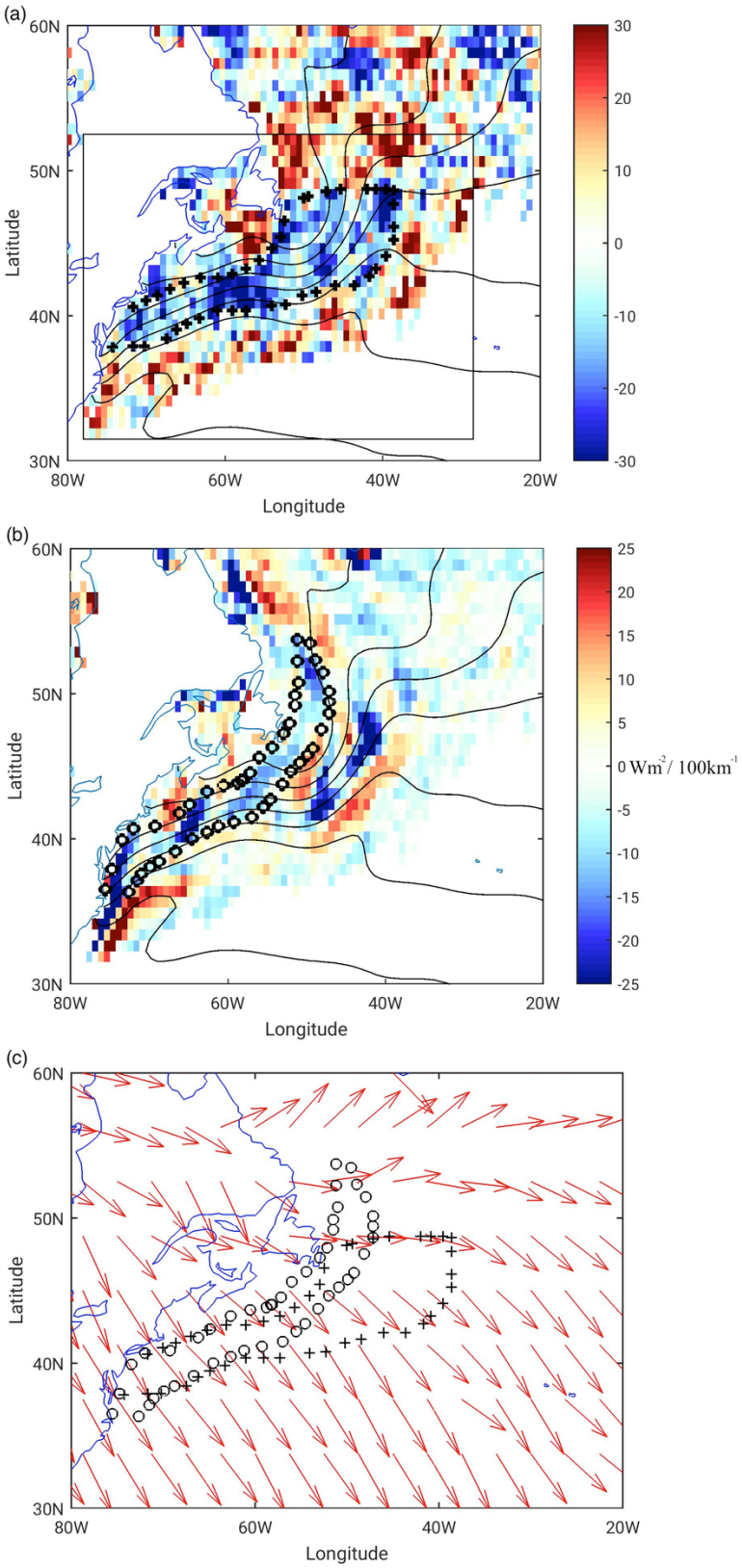

Figure S5: (a) Figure 2(d), with the addition of black stars outlining a broad region of cold frontal frequency increase (negative values) across the GS front in the High-res period. (b) Figure 3(c), with black circles outlining a broad region where there exists on average a reduced thermal damping of cold fronts in the High-res period. (c) The red arrows illustrate the average direction of the cross cold frontal temperature gradient $(-y)$ in the High-res period. The delay of up to 10^{o} between these two areas results from the timescale of thermal interaction and the natural variability of the cold fronts.

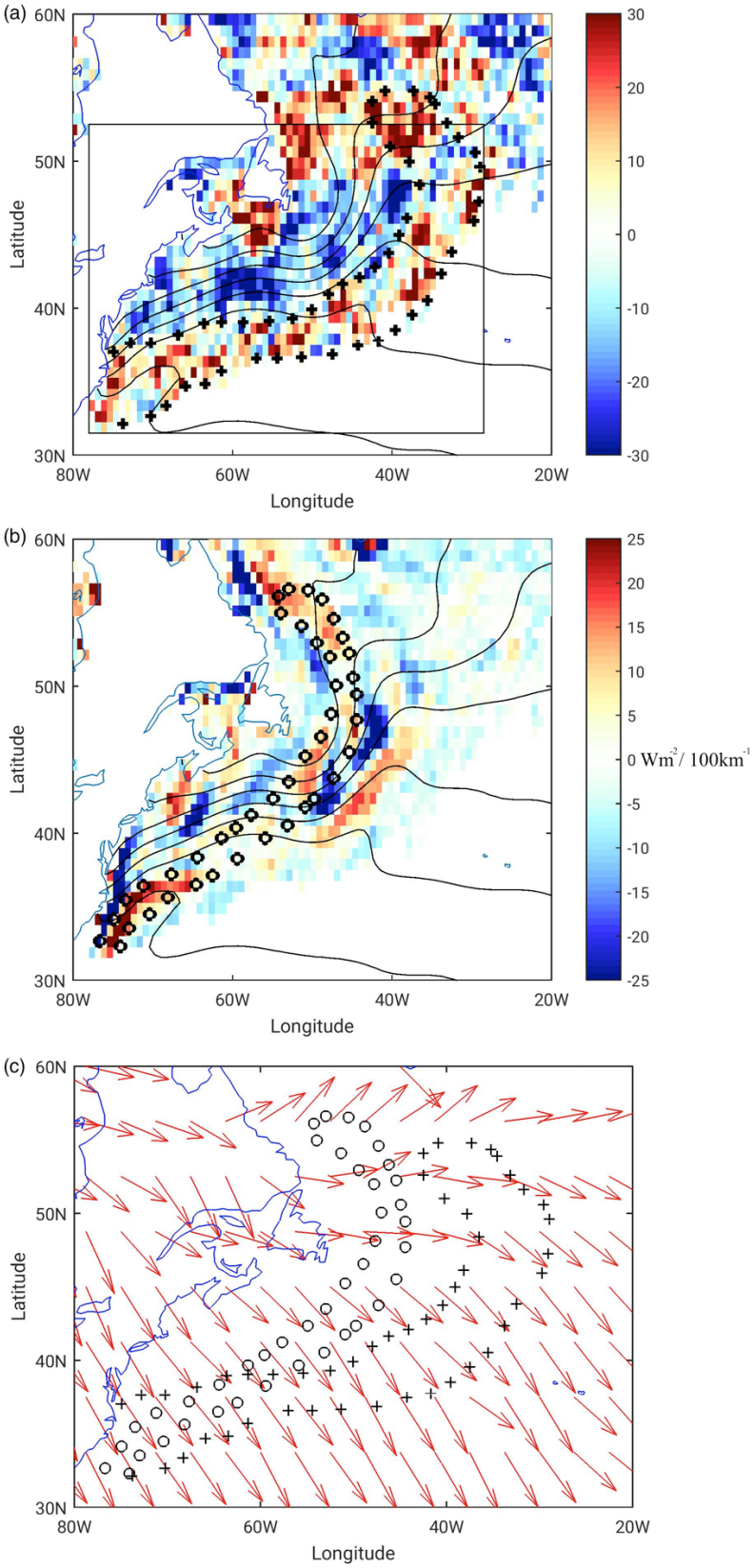

Figure S6: (a) As in Figure S5(a), but outlining a broad region of cold frontal frequency decrease (positive values) across the GS front in the High-res period. (b) As in Figure S5(b), but outlining a broad region where there exists on average an increased thermal damping of cold fronts in the High-res period. (c) As in Figure S5(c), with the regions in S6(a) and (b) highlighted instead.

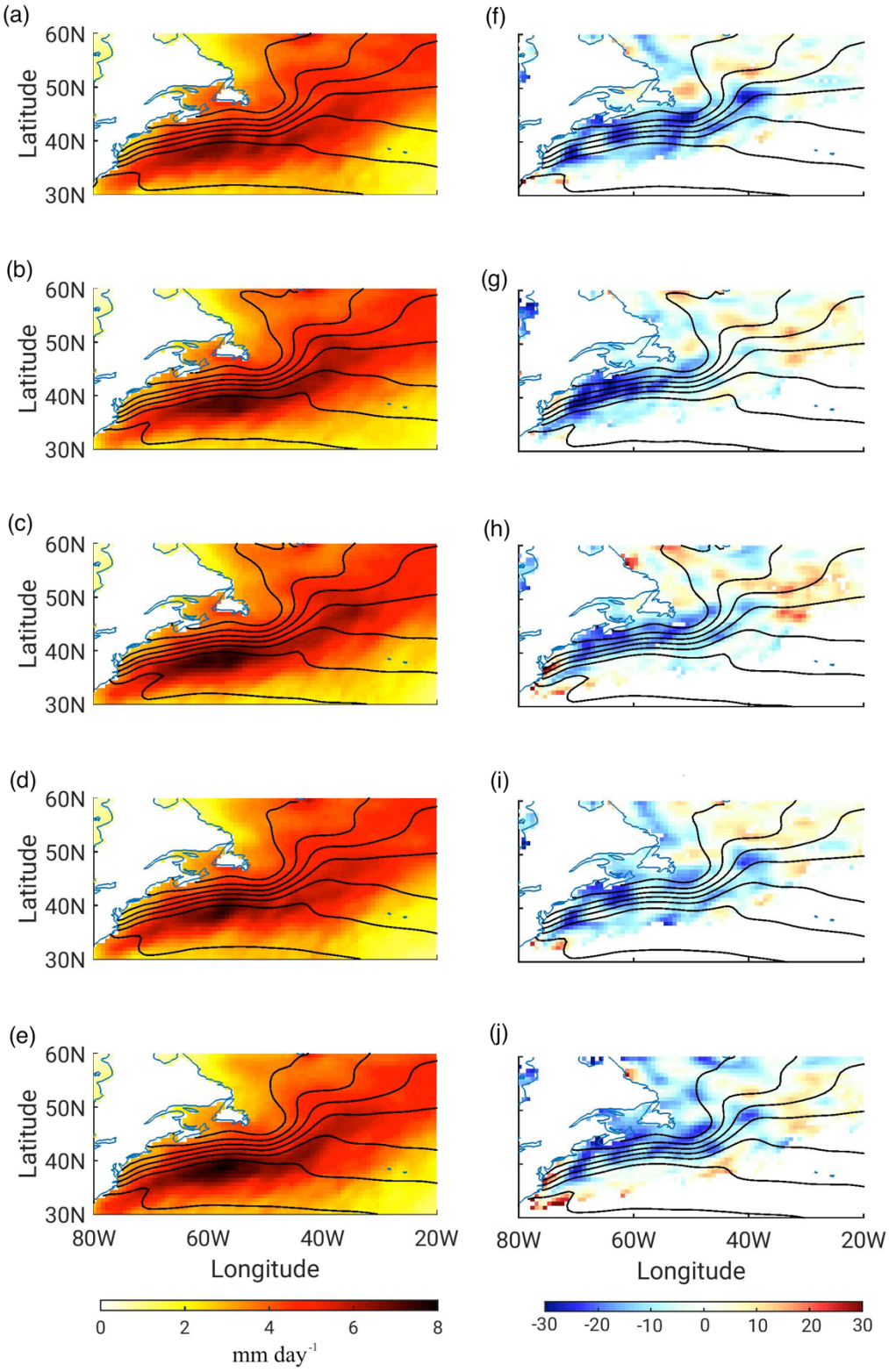

Figure S7: The mean total precipitation for (a-e) Low-res sample ii-vi, respectively. (f-j) The percentage differences between the High-res period and each six-year Low-res sample ii-vi, respectively. This difference is calculated as 100*(Low-res - High-res)/(High-res) such that negative (positive) values imply more (less) precipitation in the High-res period. The mean SST contours from each corresponding Low-res period are plotted from 3°C to 24°C, at 3°C intervals.

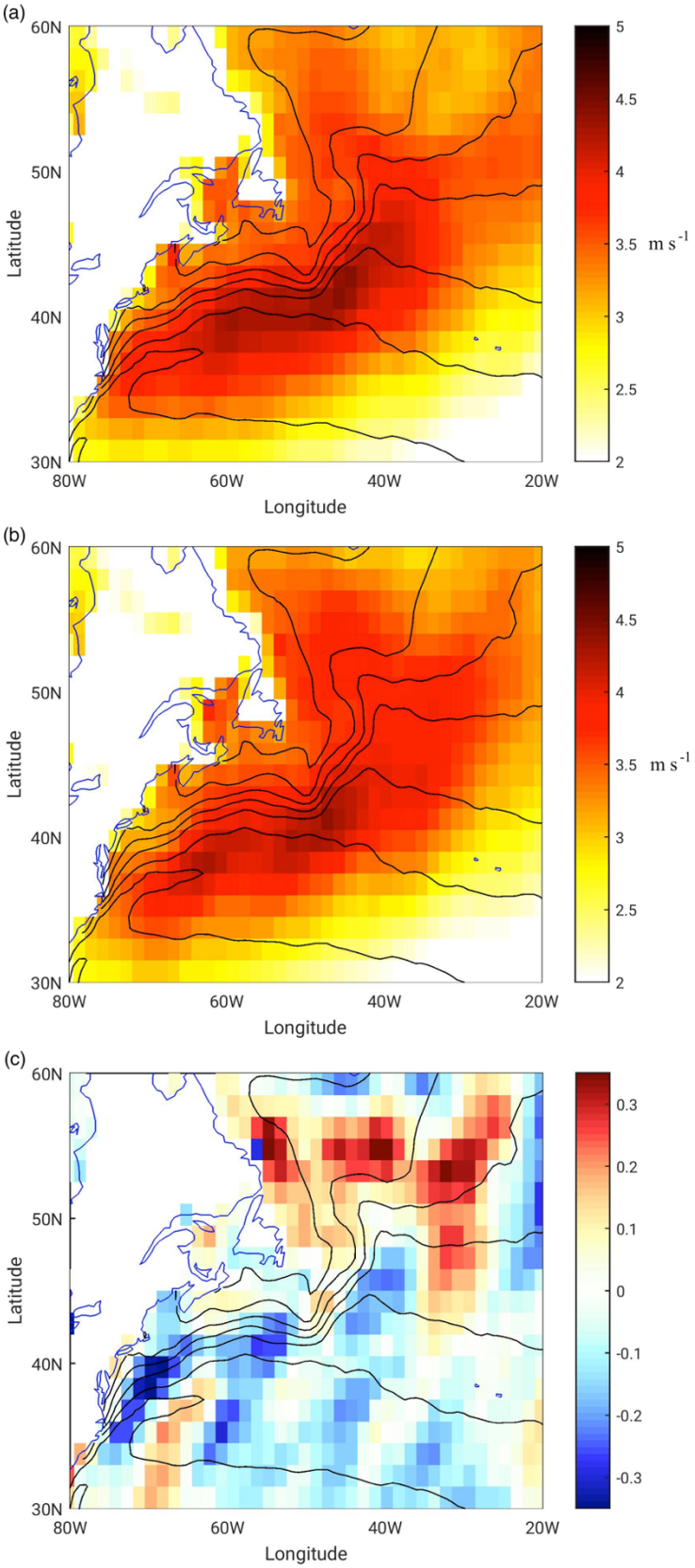

Figure S8: The mean standard deviation of the 10 m northward wind (band-passed for approximately 2-6 days using the daily difference filter following Wallace et al. (1998)) for (a) the High-res period and (b) Low-res sample *i*. (c) The absolute difference between the two periods, calculated as Low-res minus High-res, such that negative (positive) values indicate more (less) storm-track activity in the High-res period.

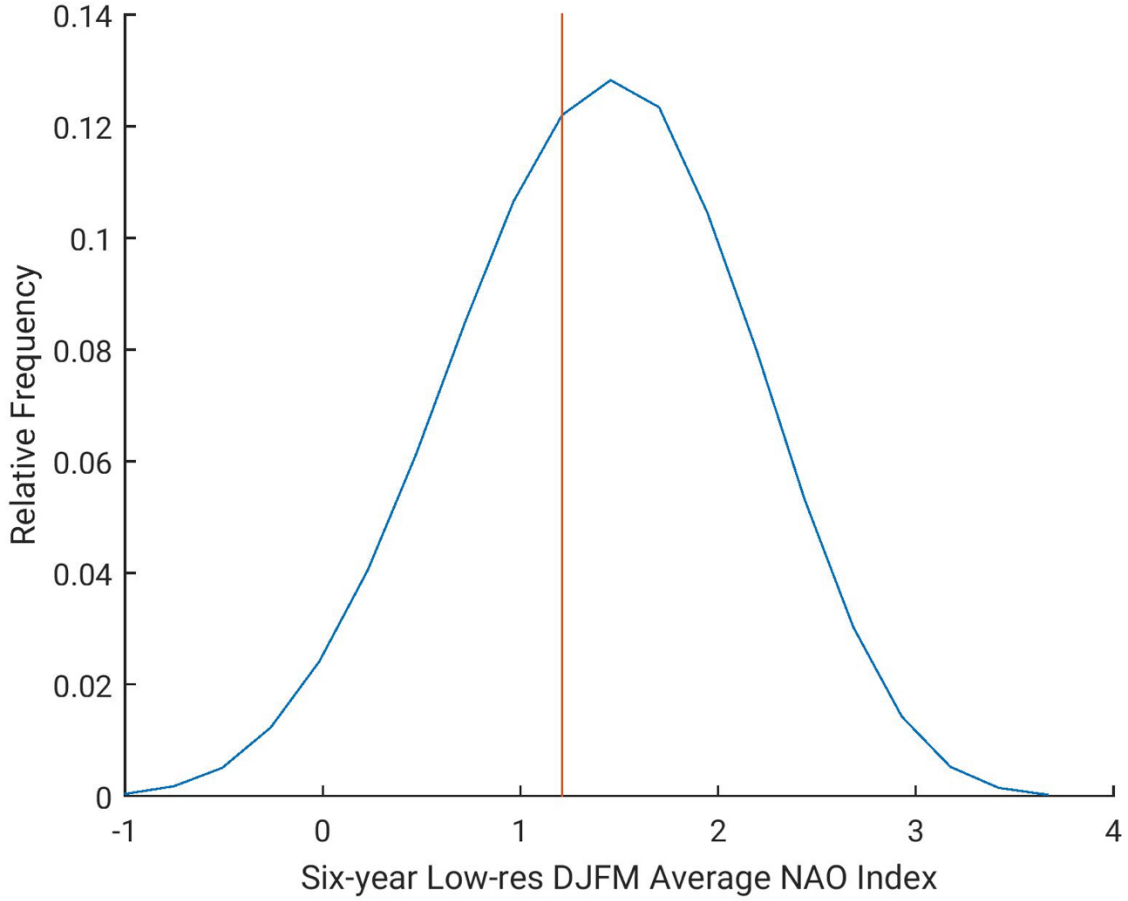

Figure S9: Histogram of all possible randomly chosen six-year averages of NAO DJFM index (Hurrell 1995; Retrieved from https://climatedataguide.ucar.edu/climate-data/hurrell-north-atlantic-oscillation-nao-index-station-based) from the Low-res period. The red line shows the six-year NAO DJFM index average for the High-res period.